Bull. Mater. Sci., Vol. 34, No. 2, April 2011, pp. 271–277. © Indian Academy of Sciences.

Synthesis of new (Bi, La)$_3$MSb$_2$O$_{11}$ phases (M = Cr, Mn, Fe) with KSbO$_3$-type structure and their magnetic and photocatalytic properties

K RAMESHA*, A S PRAKASH, M SATHIYA, GIRIDHAR MADRAS† and A K SHUKLA†
CSIR Central Electrochemical Research Institute-Madras Unit, CSIR-Madras Complex, Taramani, Chennai 600 113, India
†Solid State and Structural Chemistry Unit, Indian Institute of Science, Bangalore 560 012, India

MS received 26 October 2010; revised 14 December 2010

Abstract. **Synthesis and structure of new (Bi, La)$_3$MSb$_2$O$_{11}$ phases (M = Cr, Mn, Fe) are reported in conjunction with their magnetic and photocatalytic properties. XRD refinements reflect that Bi$_3$CrSb$_2$O$_{11}$, Bi$_2$LaCrSb$_2$O$_{11}$, Bi$_2$LaMnSb$_2$O$_{11}$ and Bi$_2$LaFeSb$_2$O$_{11}$ adopt KSbO$_3$-type structure (space group, $Pn\bar{3}$). The structure can be described through three interpenetrating networks where the first is the (M/Sb)O$_6$ octahedral network and other two are the identical networks having Bi$_6$O$_4$ composition. The magnetic measurements on Bi$_2$LaCrSb$_2$O$_{11}$ and Bi$_2$LaMnSb$_2$O$_{11}$ show paramagnetic behaviour with magnetic moments close to the expected spin only magnetic moments of Cr^{+3} and Mn^{+3}. The UV-Visible diffuse reflectance spectra are broad and indicate that these materials possess a bandgap of ∼ 2 eV. The photocatalytic activity of these materials has been investigated by degrading Malachite Green (MG) under exposure to UV light.**

Keywords. **A$_3$B$_3$O$_{11}$; KSbO$_3$; magnetism; synthesis; crystal structure; photocatalysis.**

1. Introduction

A$_3$B$_3$O$_{11}$ compounds crystallizing in KSbO$_3$-type structure exhibit interesting properties such as ionic conductivity and electrocatalysis (Gokagac and Kennedy 1993; He *et al* 1997). Both perovskite and KSbO$_3$ structures have the same chemical formula, ABO$_3$. But, unlike the perovskite structure, the KSbO$_3$ structure has characteristic tunnel arrangement, which has been ascribed to large covalent character of B–O bonds that restrict the formation of ∼ 180° B–O–B angles (Goodenough and Kafalas 1973; Hong *et al* 1974). A$_3$B$_3$O$_{11}$ is a subset / compositional variant of KSbO$_3$-family that also has the tunnel motif. A$_3$B$_3$O$_{11}$ is made up of three interpenetrating lattices (Sleight and Bouchard 1973). However, only a few members of this family are known and their physical properties have not been well studied. Sleight and Bouchard (1973) were the first to report new compounds such as Bi$_3$GaSb$_2$O$_{11}$ of A$_3$B$_3$O$_{11}$ family and observed large thermal factor for Bi. Variable temperature neutron diffraction studies showed that positional site disorder and open geometry are responsible for the observed large thermal parameters of Bi (Ismunandar *et al* 1998). Bi$_3$Ru$_3$O$_{11}$ is another important member of the family which shows Ru–Ru bonding (Abraham and Thomas 1975), while La$_3$Ru$_3$O$_{11}$ does not have direct bonding between Ru–Ru (Cotton and Rice 1978; Khalifah and Cava 2001). Recently, synthesis of a new member of this family, viz. Bi$_3$Mn$_3$O$_{11}$, is reported (Belik and Muromachi 2009). Interestingly, Bi$_3$Mn$_3$O$_{11}$ with randomly distributed Mn^{+3} and Mn^{+5} ions exhibits high ferrimagnetism with T_c at ∼ 150 K. Accordingly, A$_3$B$_3$O$_{11}$ family of oxides crystallizing in KSbO$_3$-type structure displays interesting and diverse properties owing to their remarkable structure and bonding.

Many of Sb^{+5} containing oxides such as Ca$_2$Sb$_2$O$_7$, CaSb$_2$O$_6$, NaSbO$_3$ (Abraham *et al* 1974) and AgSbO$_3$ (Singh and Uma 2009) have been investigated for their photocatalytic properties owing to their wide delocalized conduction band. Further, Bi^{+3} containing oxides Bi$_2$WO$_6$ (Sato *et al* 2002), BiVO$_4$ (Zhang and Zhu 2005), Bi$_2$Ti$_2$O$_7$ (Li *et al* 2008) exhibit photocatalytic activity on exposure to visible light. This suggests that Sb^{+5} and Bi^{+3} have the ability to induce photocatalysis in oxides. Indeed, BiSbO$_4$ (Lin *et al* 2006) shows good photocatalytic activity towards the degradation of methylene blue (MB) on exposure to both UV and visible light. Photocatalysis is a viable environmentally benign process that can be used for destruction of organic matter in effluents (Frank and Bard 1977). Malachite green (MG), a triarylmethane dye, is widely used as a biocide in the aquaculture industry as well as a dye in the silk, wool, cotton, leather, paper and acrylic industries. It is also employed as a food additive and a medical disinfectant. Despite its extensive use, MG is highly undesirable due to its toxic properties which are known to cause carcinogenesis, mutagenesis, teratogenicity and respiratory toxicity (Srivastava *et al* 2004). Recent studies have dealt with the light-induced degradation of MG by means of UV-A irradiation in TiO$_2$ aqueous suspensions (Kominami *et al* 2003), and UV-C irradiation in presence of hydrogen peroxide (Modirshahla and Behnajady 2006).

*Author for correspondence (ramesha.cecri@gmail.com)

In this study, synthesis, structure and magnetic properties of four new members of $A_3B_3O_{11}$ family adopting $KSbO_3$-type structure, viz. $Bi_3CrSb_2O_{11}$, $Bi_2LaCrSb_2O_{11}$, $Bi_2LaMnSb_2O_{11}$, and $Bi_2LaFeSb_2O_{11}$ are reported. For the purpose of comparison, we have also prepared $Bi_3FeSb_2O_{11}$ reported elsewhere (Sleight and Bouchard 1973). The study also reports the photocatalytic activity of $(Bi, La)_3MSb_2O_{11}$ oxides.

2. Experimental

2.1 *Synthesis*

Polycrystalline samples with composition $(Bi, La)_3MSb_2O_{11}$ where M = Cr, Mn, Fe were synthesized by the solid state synthesis method. Stoichiometric quantities of Bi_2O_3, La_2O_3, M_2O_3 (M = Cr, Mn or Fe) and Sb_2O_3 were mixed thoroughly and heated in air at 1000°C for 24 h followed by heating at 1100°C for 24 h with one intermediate grinding and pelletizing.

2.2 *Characterization*

X-ray powder diffraction (XRD) patterns for the oxide samples were recorded using Philips (Xpert PRO) diffractometer using CuK_α radiation. Rietveld quality data were collected with a step size of 0·02° over 12 h and refinements were carried out using General Structure Analysis System (GSAS) code (Larson and Von Dreele 2000) and EXPGUI (Toby 2001) interface. A Psuedo-Vöigt function was used to model peak profile and background was fitted with Chebyschev function.

For selected samples, magnetization measurements were carried out using PPMS (Quantum Design) magnetometer in the temperature range 5–300 K at H = 1000 Oe magnetic field. Both zero field cooled (ZFC) and field cooled (FC) data were collected. ZFC magnetic data were recorded in a field of 1000 Oe upon warming from 5K after cooling from room temperature under zero fields. FC magnetic data were also collected upon warming from 5K, but subsequently the samples were cooled under a 1000 Oe field. Magnetization versus field (M vs H) measurements were carried out at 5 K up to a maximum field of 5 Tesla.

The morphology and particle size were analysed using scanning electron microscope (JEOL-JSM-5600LV, 20 kV) attached with EDAX facility for elemental analysis. The UV-Visible diffuse reflectance spectra (DRS) for the powder sample were recorded using UV-Visible spectrometer (Lambda 32 Perkin Elmer).

2.3 *Dye materials for photodegradation studies*

Malachite green (MG) was procured from S.D. Fine Chemicals, India with more than 99% purity and was used without further purification. Water was double distilled and filtered through Millipore membrane filter prior to use.

2.4 *Photodegradation experiments*

The photocatalytic activity of compounds was studied under UV radiation. A high-pressure mercury vapour lamp (HPML) of 125 W (Philips, India) was used as UV source. The lamp radiated predominantly at 365 nm with an incident intensity of 10^{-6} Einstein L^{-1} s^{-1} and a photon flux of 25 W m^{-2}, which was measured by *o*-nitrobenzaldehyde actinometry. The design and operation of the photochemical reactor used in the study are discussed elsewhere (Aarthi and Madras 2007).

In a typical experiment, aqueous solution containing known concentration of dye (50 ppm) and catalyst (loading of 1 g/L) were taken in the photoreactor. The suspended catalyst and dye solutions were continuously stirred with a magnetic stirrer. The pH of the solution was not adjusted during the experiment and the experiments were conducted at the natural pH. The degradation under UV light in presence of the catalyst was carried out for 1 h during which samples were collected at regular intervals of time.

The collected samples were then filtered and centrifuged to remove any catalyst particles before the UV-Visible analysis. All dyes were analysed with a UV-Visible spectrometer (Lambda 32 Perkin-Elmer) between 200 and 800 nm. The calibration was based on the Beer–Lambert law at their maximum absorption wavelength, λ_{max}.

Experiments were initially conducted only with UV without any catalyst (photolysis) and with catalyst without any UV exposure (dark), and no degradation was observed in these cases. All experiments were conducted thrice and the average difference in concentration was less than ±2 ppm.

3. Results and discussion

3.1 *Phase identification and XRD Rietveld refinements*

Figure 1 shows the XRD patterns for $(Bi, La)_3MSb_2O_{11}$ phases where M = Cr, Mn, Fe. Preliminary indexing and phase identification reveal the formation of single phases with $KSbO_3$ type structure. Further, Rietveld refinements were carried out using $Bi_3GaSb_2O_{11}$ as model structure (Sleight and Bouchard 1973; Ismunandar *et al* 1996) with space group $Pn\bar{3}$. In $Bi_3GaSb_2O_{11}$, the six atoms have the following positions: Bi(1) at 8*e*(x, x, x), Bi(2) at 4*b*(0, 0, 0), Ga/Sb at 12*g* (x, ¾, ¼), O(1) at 8*e* (x, x, x), O(2) at 12*f* (x, ¼, ¼) and O(3) at 24h (x, y, z). For La containing compositions, best Rietveld fit were obtained when La was disordered at both Bi(1) and Bi(2) positions with equal site occupancy. Distributing all La at 4*b* position resulted in higher agreement factors. So Bi atoms occupying both 8*e* and 4*b* positions is crucial for stabilizing the structure. This was further confirmed by our attempts to prepare $BiLa_2MSb_2O_{11}$

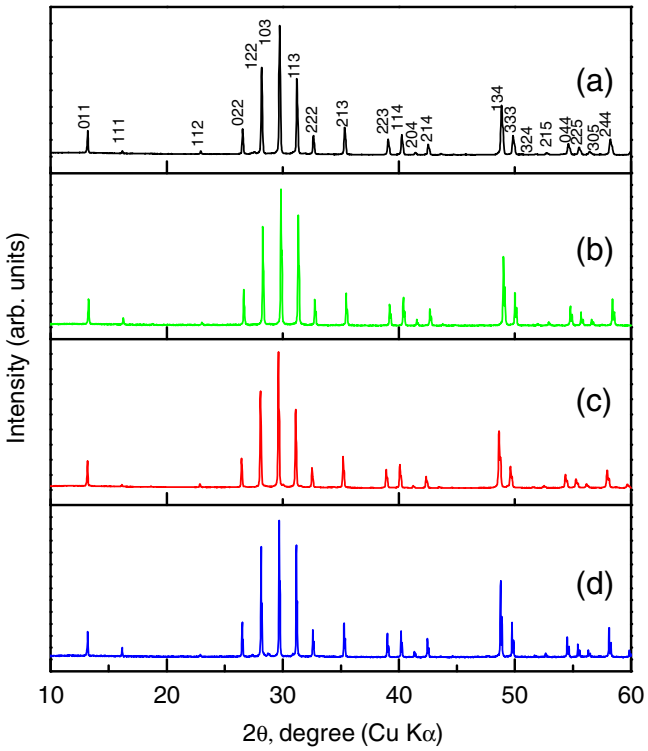

Figure 1. Powder X-ray diffraction patterns for compounds crystallizing in $KSbO_3$-type structure: (a) $Bi_2LaCrSb_2O_{11}$, (b) $Bi_3CrSb_2O_{11}$, (c) $Bi_2LaMnSb_2O_{11}$ and (d) $Bi_2LaFeSb_2O_{11}$. (*hkl*) indexing of peaks is shown in the top panel.

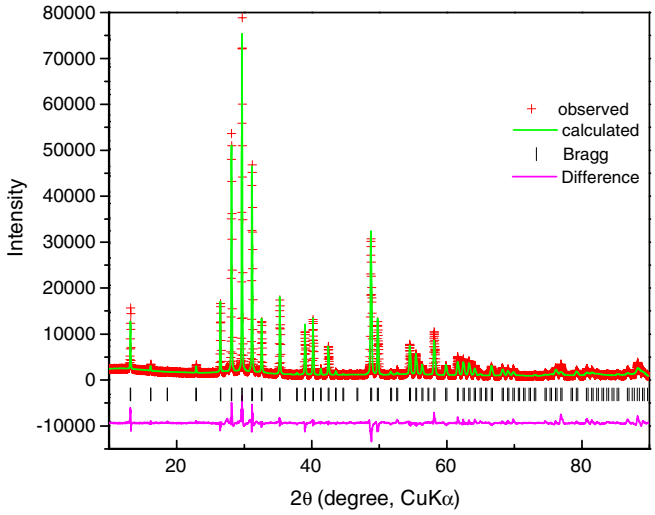

Figure 2. Powder XRD Rietveld fit for $Bi_2LaCrSb_2O_{11}$.

compounds by increasing La content in lieu of Bi, which resulted in additional impurity phases. The Rietveld fit for $Bi_2LaCrSb_2O_{11}$ is shown in figure 2 as a representative example. The crystallographic data and bond lengths are given in tables 1 and 2. The lattice parameters of all the compositions obtained from XRD Rietveld refinements are listed in table 3.

Table 1. Crystallographic data for $Bi_2LaCrSb_2O_{11}$.

Atom	Position	x	y	z	B (Å)^2
Bi(1)	8e	0·3821	0·3821	0·3821	1·22(3)
Bi(2)	4b	0	0	0	0·94(2)
Cr, Sb	12g	0·5949	0·75	0·25	0·63(2)
O1	8e	0·1367	0·1367	0·1367	0·84(3)
O2	12g	0·6023	0·25	0·25	0·78(3)
O3	24h	0·5937	0·5314	0·2471	0·67(1)

Cubic, space group $Pn\bar{3}$, $a = 9{\cdot}506(3)$ Å, $R_{wp} = 8{\cdot}81$, $\chi^2 = 3{\cdot}44$.

Table 2. Interatomic distances (Å) for $Bi_2LaCrSb_2O_{11}$.

Bi1–O1 (×3)	2·346(1)	Cr/Sb–O2 (×2)	2·036(1)
Bi1–O2 (×3)	2·745(1)	Cr/Sb–O3 (×2)	2·070(1)
Bi1–O3 (×3)	2·776(1)	Cr/Sb–O3 (×2)	1·910(1)
Bi2–O1 (×2)	2·251(1)		
Bi2–O3 (×6)	2·529(2)		

Table 3. Lattice parameters for (Bi, La)$_3$MSb$_2$O$_{11}$ compounds.

Compound	Lattice parameter, a (Å)
$Bi_2LaCrSb_2O_{11}$	9·506(3)
$Bi_3CrSb_2O_{11}$	9·478(2)
$Bi_2LaMnSb_2O_{11}$	9·546(2)
$Bi_2LaFeSb_2O_{11}$	9·523(3)
$Bi_3FeSb_2O_{11}$	9·516(3)

Our efforts to synthesize $Bi_3MnSb_2O_{11}$ and $Bi_3NiSb_2O_{11}$ in $KSbO_3$ type structure were unsuccessful. Instead, pyrochlore phases (Ramesha *et al* 2003a, b) were obtained as revealed from their powder XRD patterns. The formation of pyrochlore phase implies that Mn is in +2 oxidation state (instead of +3) corresponding to the chemical formula, $Bi_2Mn_{0{\cdot}67}Sb_{1{\cdot}33}O_7$.

3.2 *Crystal structure*

The structure essentially can be viewed as three interpenetrating networks (figure 3). The M and Sb form octahedral network with oxygen similar to that found in $KSbO_3$. The MSb_2O_9 array consists of pair of edge sharing octahedra and every such unit is further connected through vertices to form 3-dimensional network (figure 3a). The other two identical networks (figure 3b) contain only Bi and O1 atoms. Four Bi(2) atoms form a tetrahedron that contain O(1) on every face. The Bi(1) atom is connected to two such tetrahedron through O(1). Two such networks with a formula, $Bi(2)_4O(1)_4Bi(1)_2$, interpenetrate the MSb_2O_9 octahedral network. The entire Bi-oxygen network can also be described as corner sharing Bi_8O_4 stellate quadrangulae formed by four $Bi(1)_3Bi(2)$ tetrahedra each containing O1, in

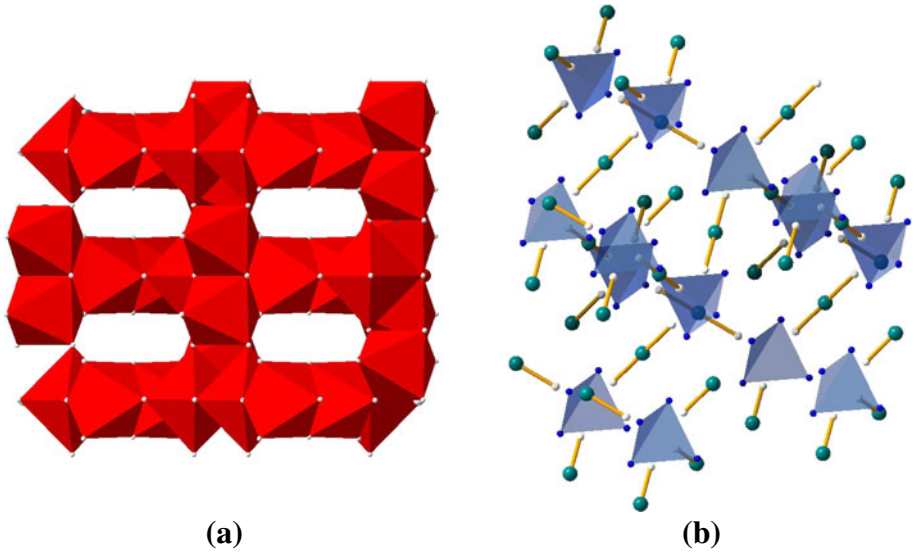

Figure 3. Crystal structure of (Bi, La)$_3$MSb$_2$O$_{11}$ showing interpenetrating networks. **(a)** MSb$_2$O$_{11}$ octahedral network with M–Sb atoms at the centre and oxygen atoms at corners of octahedra, **(b)** two identical Bi$_6$O$_4$ networks where Bi(2) atoms (blue) form tetrahedron that contain O(1) atom (white) on every face. The Bi(1) atoms (green) are connected to two such tetrahedron through O(1).

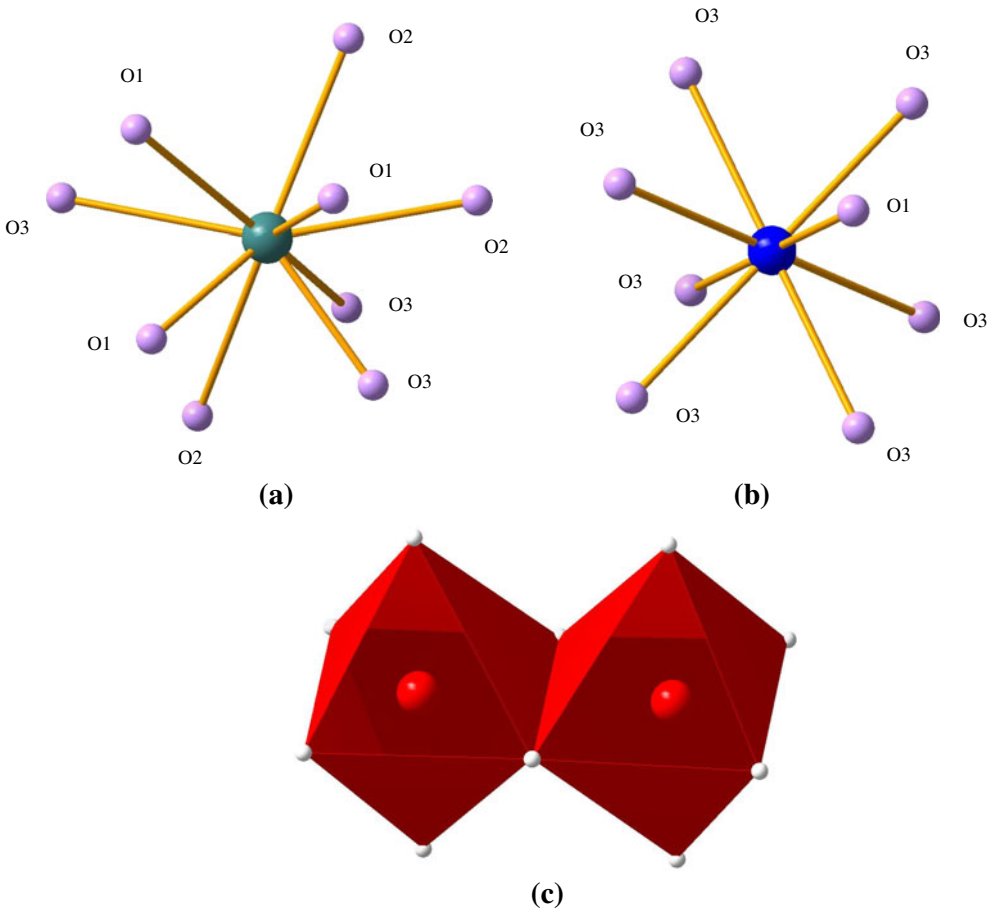

Figure 4. Ball-and-stick drawing for **(a)** the coordination of Bi(1)O$_9$ polyhedron, **(b)** Bi(2)O$_8$ coordination and **(c)** edge shared (MSb$_2$)O$_9$ octahedra.

turn sharing Bi(1)$_3$ face with fifth empty Bi(1)$_4$ tetrahedron (Ismunandar *et al* 1996).

Figure 4 shows the ball-and-stick drawing of the oxygen coordination sphere around Bi(1), Bi(2) and (M/Sb$_2$). Bi(1) atoms connected to 9 oxygen atoms form a tricapped trigonal prism while Bi(2) has 8-fold coordination similar to that found in pyrochlores. The structure of $Bi_3GaSb_2O_{11}$ has been discussed in detail elsewhere (Sleight and Bouchard 1973; Ismunandar *et al* 1996). In contrast to the $Bi_3GaSb_2O_{11}$ structure, the O1 atoms are absent in $KSbO_3$ and K atoms lie in the cavity formed by SbO_3 framework.

3.3 *Magnetic properties*

In (Bi, La)$_3$MSb$_2$O$_{11}$ (M = Cr, Mn, Fe) compositions, only M atoms are the magnetic species, which are statically distributed in the MSb$_2$O$_9$ network. Accordingly, only paramagnetic behaviour can be expected. The χ_M^{-1} vs T plots for $Bi_2LaCrSb_2O_{11}$ and $Bi_2LaMnSb_2O_{11}$ are shown in figure 5 with M vs H behaviour at 5 K in the inset. As expected, the χ_M^{-1} vs T behaviour is linear for both the compounds, confirming paramagnetic interaction. The ZFC and FC data converge, and there is no separation between FC and ZFC curves down to 5K. For Cr composition, the plot is linear (figure 5a) and fits well to Curie behaviour ($\theta = 0$) in the temperature range 5–280K. The spin-only magnetic moment obtained is 3·65 μ_B which is slightly smaller than calculated spin-only moment for 3 unpaired spins; expected μ_{eff} for Cr^{+3} being 3·9 μ_B. The χ_M^{-1} vs T plot for Mn composition (figure 5b) follows Curie–Weiss law. A linear fit between 50 K and 300 K yields $\theta = -7{\cdot}4$ K, and $\mu_{eff} = 4{\cdot}7\ \mu_B$; the calculated μ_{eff} value for spin-only Mn^{3+} (d^4) being 4·9 μ_B. There is a small deviation of slope below 10 K with θ becoming zero. The M vs H plots at 5 K (insets to figures 5a–b) are typical Brillouin functions for the magnetization of paramagnets.

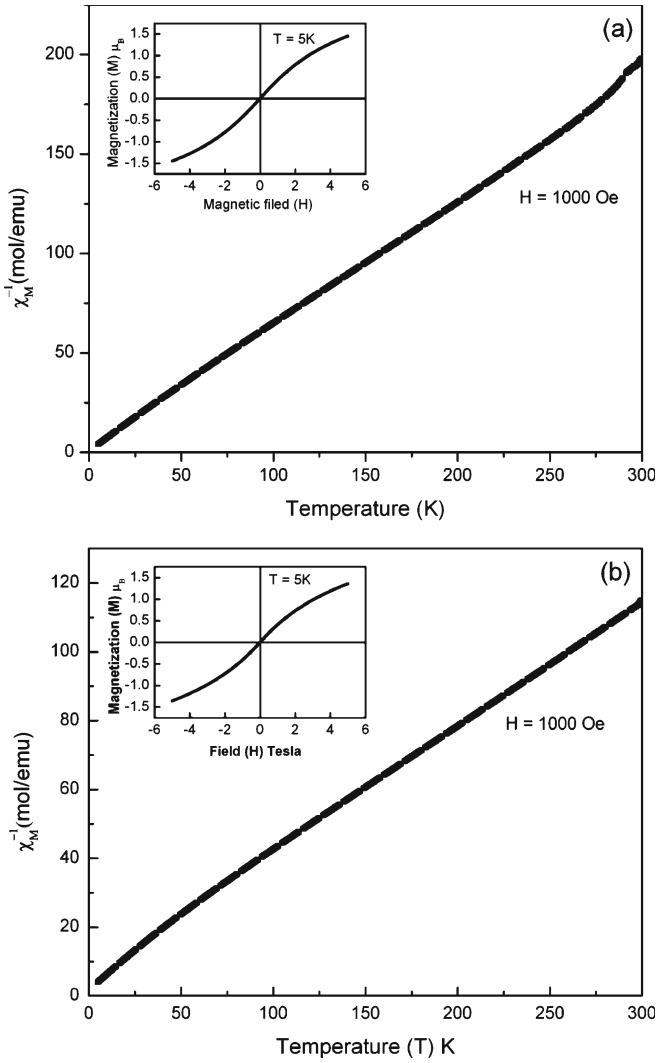

Figure 5. χ_M^{-1} vs T plots for (a) $Bi_2LaCrSb_2O_{11}$ and (b) $Bi_2LaMnSb_2O_{11}$. The M vs H data at 5K are shown as inset.

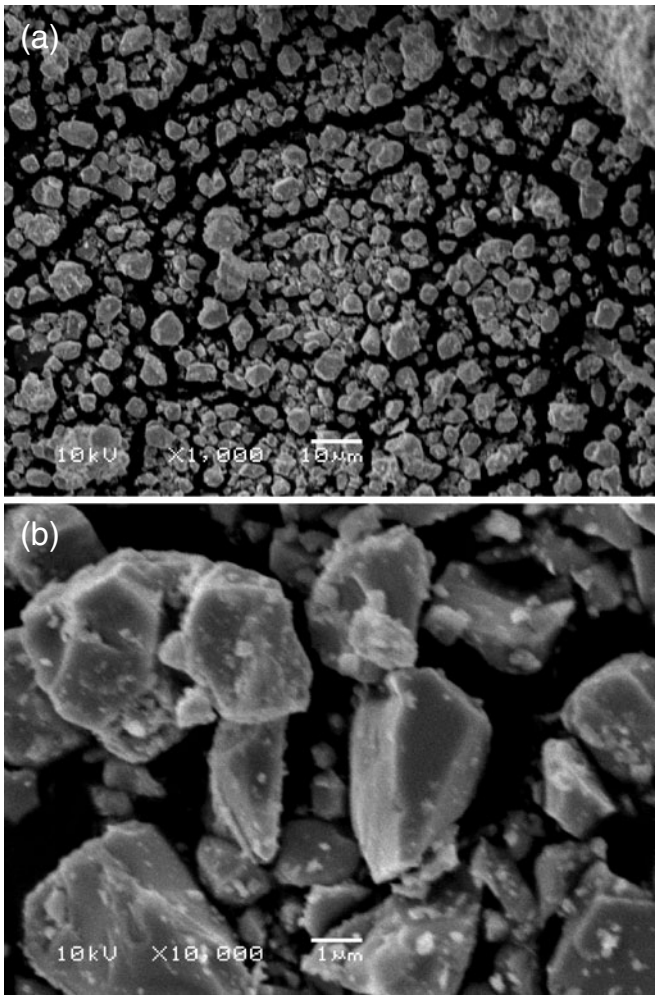

Figure 6. SEM micrographs for $Bi_2LaMnSb_2O_{11}$ at two different magnifications.

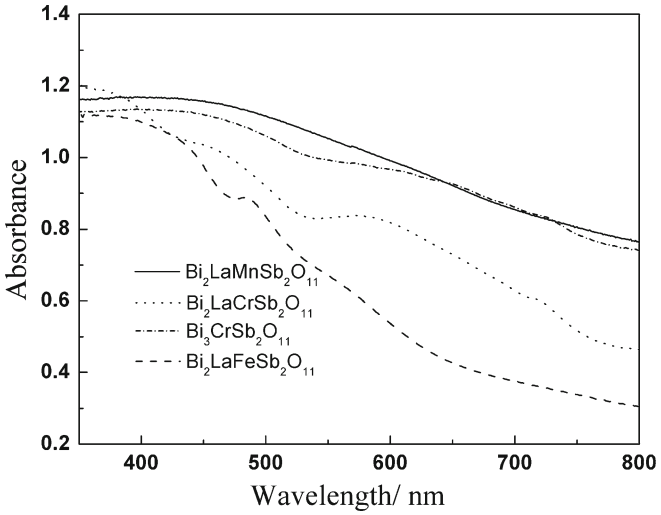

Figure 7. UV-Vis diffuse-reflectance spectra for $(Bi, La)_3MSb_2O_{11}$ (M = Cr, Mn, Fe) compounds.

3.4 *SEM and DRS*

The scanning electron micrographs for $Bi_2LaMnSb_2O_{11}$ phase are shown in figures 6(a) and (b). The micron-sized particles are depicted in the micrographs. The EDAX spectrum recorded on various crystallites confirms the cation stoichiometry. Figure 7 shows the diffuse-reflectance spectra (DRS) of the members. DRS reveals that $(Bi, La)_3MSb_2O_{11}$ compounds show broad absorption in the UV-Visible range similar to that found for $BiVO_4$ (Kudo *et al* 1999), $BiCu_2VO_6$ (Liu *et al* 2005), Ag_2CrO_4 (Ouyang *et al* 2008), $CsLaSrNb_2NiO_9$ (Yao and Ye 2006) oxides, which are excellent photocatalysts. It is noteworthy that the onset of absorption edges (figure 7) is unclear because of several absorption overlaps in the visible range. For instance, the spectra for $Bi_2LaFeSb_2O_{11}$ indicate that there would be more than two absorption edges with main absorption edge at around 600 nm ($E_g = 2{\cdot}07$ eV). In addition, there are two more absorption edges around 630 nm ($E_g = 1{\cdot}97$ eV) and 700 nm ($E_g = 1{\cdot}77$ eV). Similarly two absorption edges could be identified for $Bi_2LaCrSb_2O_{11}$ at 670 nm (1·85 eV) and 710 nm (1·75 eV).

The band structure of oxides is generally defined by metal d-level and O $2p$ level, the valence band is assumed to be O $2p$ level and the metal d-levels constitute the conduction band (Scaife 1980). Absorption of photons with an energy equal to or greater than bandgap generates electron–hole pairs. When oxides contain transition metals with partially filled d-orbitals, the electronic structure is strongly influenced by the transition metals (Wang *et al* 2003; Yao and Ye 2006). The visible light response of such compounds is attributed to the splitting of d-orbitals in octahedral field that creates new band levels in the bandgap (Wang *et al* 2003; Yin *et al* 2003). The two or more absorption edges observed in the DRS spectra of $Bi_2LaFeSb_2O_{11}$ or $Bi_2LaCrSb_2O_{11}$ indicate that additional energy levels have been created due to the partially filled d-orbitals of Fe^{+3} or Cr^{+3}. From the band structure of Bi^{+3} and Sb^{+5} containing compounds (Lin *et al* 2006), one can constitute the band structure of $(Bi, La)_3MSb_2O_{11}$ compounds as follows: the valence band mainly composed of O$2p$ orbitals hybridized by Bi $6s$ and Sb $4d$ orbitals. The conduction band primarily consists of Sb $5s$ and Bi $6p$ orbitals. The hybrid states in valence band as well as conduction band and their s character imply a high mobility of photogenerated charge carriers favouring photocatalytic property (Kim *et al* 2004; Tang *et al* 2007).

3.5 *Photocatalysis*

MG is a non-volatile and highly soluble compound and hydroxyl radical mediated reactions are likely to occur primarily in the liquid bulk. Because these reactions occur at relatively low substrate concentrations, they can usually be described by a pseudo-first order kinetic expression:

$$\frac{dC}{dt} = kt.$$

The above relationship can be solved to obtain $C/C_0 = e^{-kt}$ where C is the concentration of the dye, C_0 the initial concentration of the dye, t the time and k the rate constant. The degradation profile for the dye and the degradation rate constant are shown in figure 8. It is clear that the dye is degraded in presence of the catalyst. It is also clear that the degradation in presence of $Bi_2LaMnSb_2O_{11}$ is highest.

The photocatalytic property depends on the crystal structure. Tunnel structures or distorted structures generally

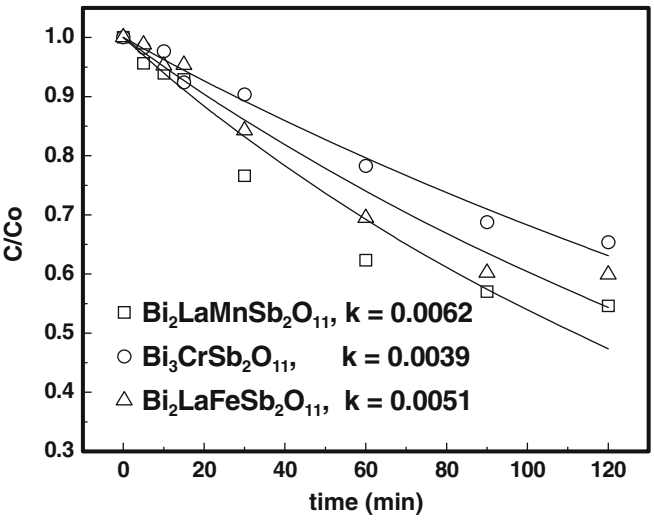

Figure 8. Degradation profile of Malachite green (MG) dye in presence of catalyst material $Bi_2LaMnSb_2O_{11}$, $Bi_3CrSb_2O_{11}$ and $Bi_2LaFeSb_2O_{11}$ under UV light. C_0 is the initial concentration and C the concentration at time, t. The lines fitted by the first order rate and the rate constant (k) are also indicated.

promote catalytic property as for $BaTi_4O_9$ and $A_2Ti_6O_{13}$ (A = Na, K) compounds (Templeton and Dauben 1960; Hofmeister *et al* 1984; Kohno *et al* 2000). Such structures possess dipole moment that facilitates photogeneration of carriers, their efficient separation and transport. Accordingly, the photocatalytic property of (Bi, La)$_3$MSb$_3$O$_{11}$ compounds can be related to their tunnel structure that contains highly distorted (M/Sb)O_6, Bi(1)O_9 and Bi(2)O_8 polyhedra. For instance, in $Bi_2LaCrSb_2O_{11}$ there are three types of Bi(1)–O distances (2·346, 2·745, 2·776 Å) and two types of Bi(2)–O distances (2·251, 2·529 Å). The (Cr/Sb)$_2O_9$ units that form three-dimensional tunnel structure consists of a pair of edge sharing distorted (Cr/Sb)O_6 octahedra, which exhibit three types of Cr/Sb-O bond distances (2·036, 2·070 and 1·910 Å). The presence of such distorted units induces dipole moment in the structure, which enables formation of photo-generated charge carriers and their effective separation (Sato *et al* 2002; Lin *et al* 2006). In addition, the hybrid nature of valence band and conduction band also favours the high mobility of charge carriers (Tang *et al* 2007).

4. Conclusions

New members of $A_3B_3O_{11}$ family with composition (Bi, La)$_3$MSb$_2$O$_{11}$ are synthesized and their structure determined by XRD Rietveld refinements. $Bi_3CrSb_2O_{11}$, $Bi_2LaCrSb_2O_{11}$, $Bi_2LaMnSb_2O_{11}$, and $Bi_2LaFeSb_2O_{11}$ compositions adopt $KSbO_3$-type structure. The magnetic measurements on $Bi_2LaCrSb_2O_{11}$ and $Bi_2LaMnSb_2O_{11}$ samples showed paramagnetic behaviour. The observed μ_{eff} values are 3·65 and 4·7 μ_B, respectively which are close to the calculated spin-only moments for Cr^{+3} (d^3) and Mn^{+3}(d^4) ions. $Bi_3MnSb_2O_{11}$ and $Bi_3NiSb_2O_{11}$ do not form $KSbO_3$-type structure and, instead, adopt pyrochlore phases. The photocatalytic properties of (Bi, La)$_3$MSb$_2$O$_{11}$ compounds are investigated by degrading a dye, Malachite green, under UV light. The study indicates that compounds studied here are photocatalytically active.

References

Aarthi T and Madras G 2007 *Ind. Eng. Chem. Res.* **46** 7

Abraham F and Thomas D 1975 *Bull. Soc. Fr. Mineral Crystallogr.* **98** 25

Abraham F, Nowogrocki G and Thomas D 1974 *C.R. Seances Acad. Sci., Ser. C* **278** 421

Belik A A and Muromachi E T 2009 *J. Am. Chem. Soc.* **131** 9504

Cotton F A and Rice C E 1978 *J. Solid State Chem.* **25** 137

Frank S N and Bard A J 1977 *J. Am. Chem. Soc.* **99** 303

Gokagac G and Kennedy B J 1993 *Langmuir* **9** 1862

Goodenough J B and Kafalas J K 1973 *J. Solid State Chem.* **6** 493

He L, Anderson J, Franzen H F and Johnson D C 1997 *Chem. Mater.* **9** 715

Hofmeister W, Tillmanns E and Bauer W H 1984 *Acta Crystallogr.* **C40** 1510

Hong H Y-P, Kafalas J A and Goodenough J B 1974 *J. Solid State Chem.* **9** 345

Ismunandar, Kennedy B J and Hunter B A 1996 *J. Solid State Chem.* **127** 178

Ismunandar, Kennedy B J and Hunter B A 1998 *Solid State Commun.* **108** 649

Khalifah P and Cava R J 2001 *Phys. Rev.* **B64** 085111

Kim H G, Hwang D W and Lee J S 2004 *J. Am. Chem. Soc.* **126** 8912

Kohno M, Ogura S, Sato K and Inoue Y 2000 *Chem. Phys. Lett.* **319** 451

Kominami H, Kumamoto H, Kera Y and Ohtani B 2003 *J. Photochem. Photobiol.* **A160** 99

Kudo A, Omori K and Kato H 1999 *J. Am. Chem. Soc.* **121** 11459

Larson A C and Von Dreele R B 2000 Los Alamos National Laboratory Report No. LAUR86-748

Li G, Zhang D and Yu J C 2008 *Chem. Mater.* **20** 3983

Lin X P, Huang F U, Wang W D and Zhang K L 2006 *Appl. Catal.* **A307** 257

Liu H, Nakamura R and Nakato Y 2005 *Chem. Phys. Chem.* **6** 2499

Modirshahla N and Behnajady M A 2006 *Dyes Pigments* **70** 54

Ouyang S, Li Z, Ouyang Z, Yu T, Ye J and Zou Z 2008 *J. Phys. Chem.* **C112** 3134

Ramesha K, Sebastian L, Eichhorn B and Gopalakrishnan J 2003a *J. Mater. Chem.* **13** 2011

Ramesha K, Sebastian L, Eichhorn B and Gopalakrishnan J 2003b *Chem. Mater.* **15** 668

Sato J, Saito N, Nishiyama H and Inoue Y 2002 *J. Photochem. Photobiol.* **A148** 85

Scaife D E 1980 *Sol. Energy* **25** 41

Singh J and Uma S 2009 *J. Phys. Chem.* **C 113** 12483

Sleight A W and Bouchard R 1973 *Inorg. Chem.* **12** 2314

Srivastava S, Sinha R and Roy D 2004 *Aquat. Toxicol.* **66** 319

Tang J, Zou Z and Ye J 2007 *J. Phys. Chem.* **C111** 12779

Templeton D H and Dauben C H 1960 *J. Chem. Phys. Lett.* **32** 1515

Toby B H 2001 *J. Appl. Crystallogr.* **34** 210

Wang W, Zou Z and Ye J 2003 *Chem. Phys. Lett.* **373** 191

Yao W and Ye J 2006 *Catal. Lett.* **110** 139

Yin J, Zou Z and Ye J 2003 *J. Phys. Chem.* **B107** 4936

Zhang C and Zhu Y 2005 *Chem. Mater.* **17** 3537